This is the peer reviewd version of the followng article:

Ambient vibration-based finite element model updating of an earthquake-damaged masonry tower / Bassoli, Elisa; Vincenzi, Loris; D'Altri, Antonio Maria; De Miranda, Stefano; Forghieri, Marianna; Castellazzi, Giovanni. - In: STRUCTURAL CONTROL & HEALTH MONITORING. - ISSN 1545-2255. - 25:5(2018), pp. e2150-e2150. [10.1002/stc.2150]

Terms of use:

The terms and conditions for the reuse of this version of the manuscript are specified in the publishing policy. For all terms of use and more information see the publisher's website.

09/01/2026 03:29

(Article begins on next page)

Received <day> <Month>, <year>; | Revised <day> <Month>, <year>; | Accepted <day> <Month>, <year>

DOI: xxx/xxxx

RESEARCH ARTICLE

Ambient vibration-based Finite Element model updating of an earthquake-damaged masonry tower

Elisa Bassoli[1] | Loris Vincenzi[1] | Antonio Maria D'Altri[2] | Stefano de Miranda[2] | Marianna Forghieri[1] | Giovanni Castellazzi[2]

[1]Department of Engineering "Enzo Ferrari" (DIEF), University of Modena and Reggio Emilia, Italy

[2]Department of Civil, Chemical, Environmental, and Materials Engineering (DICAM), University of Bologna, Italy

Correspondence

*Elisa Bassoli, Via Vivarelli 10, 41125, Modena, Italy Email: elisa.bassoli@unimore.it

Abstract

This paper presents a vibration-based model updating procedure for historical masonry structures which have suffered severe damage due to seismic events. This allows gathering in-depth insights on the current condition of damaged buildings, which can be beneficial for the knowledge of their actual structural behaviour and, consequently, for the design of repairing and strengthening interventions. The methodology, based on the experimentally identified modal parameters, is tested on the San Felice sul Panaro medieval fortress, which was heavily damaged by the 2012 Emilia earthquake. The Finite Element (FE) mesh of the structure in its post-quake condition is generated by means of a non-standard semi-automatic mesh generation procedure based on a laser scanner points cloud. Ambient vibration testing is performed on the main tower of the fortress. Mechanical properties of the tower and the level of connections with the rest of the fortress in its current damaged state are investigated. To fully characterize the actual behaviour of the tower in operational conditions, mesh elements corresponding to the damaged masonry are identified and different material properties are assigned to them. This allows to account for the effect of damage and cracks, which appeared essential in the calibration process. The updating procedure is carried out by means of an advanced surrogate-assisted evolutionary algorithm designed for reducing the computational effort.

KEYWORDS:

Masonry; Ambient vibration testing; Model calibration; Damaged material

1 | INTRODUCTION

From the ancient times, many masonry buildings have been damaged by earthquakes[1]. Focusing, for instance, on the Italian territory, the seismic events recorded in the last 10 years caused significant damage, in many cases up to collapse, in thousands of historical masonry structures[2].

Generally, heritage buildings have been conceived to bear static gravitational loads only, and they mostly present a low aptitude to resist toward earthquakes. This is further emphasized by the poor strength of ancient masonry against horizontal loads, where mortar joints act as planes of weakness[3]. Indeed, cracking of units and mortar, as well as shear-slip and tensile-cracking of unit-mortar interfaces have been widely recorded in post-quake surveys of ancient buildings[4].

The disasters caused by recent earthquakes motivated the scientific community in developing innovative strengthening systems for masonry constructions[5,6,7]. Nevertheless, the understanding of the weaknesses of historical masonry buildings and, therefore, the design of effective strengthening interventions is a challenging task[8,9,10,11]. Numerical modelling approaches appear to be reliable tools aiming at helping the knowledge of the structural behaviour of historical buildings[12] and at evaluating the effectiveness of retrofitting designs[13]. Indeed, accurate Finite Element (FE) models that can describe the actual structural behaviour are of great importance for evaluating the seismic response, assessing post-earthquake conditions, simulating the effects of structural modifications or repair interventions and monitoring the structural health[14,15].

Although significant advances have been achieved in this field, the understanding of the actual behaviour of historical buildings still presents a high level of uncertainty, which is related to complex geometries, mechanical properties, boundary conditions, interaction between adjacent parts, etc. When dealing with structures that have suffered severe damage due to seismic or other catastrophic events, the presence of damage, the partial collapse of some sub parts and the degradation of local and global stiffness make the characterization of the structural behaviour even more complicate.

In this field, Ambient Vibration Testing (AVT) and vibration-based structural identification are well-known non-destructive methodologies aimed at assessing the structural conditions of historical buildings. They rely on the identification of structural dynamic characteristics from output-only records using Operational Modal Analysis (OMA) techniques[16]. The vibration-based structural assessment includes full-scale ambient vibration testing[17,18,19], modal identification from ambient vibration response[20,21,22], finite element modelling and identification of the uncertain structural parameters of the model[23,24,25]. Results from AVT allow to define reliable finite element models to be used for the seismic assessment of historical constructions (see for instance[26]).

AVT has been successfully adopted to assess the current global behaviour of historical structures in several applications. Many of these applications involve masonry towers and have multiple goals, such as structural identification[27], seismic assessment[26], evaluation of the bell swinging effects[28], evaluation of the reinforcing intervention effectiveness[29,30] and damage assessment[31,32]. Some investigations related to arched structures[33], churches and monuments[34,35] can also be found in literature.

Furthermore, AVT and calibrated FE models are of great importance for evaluating the modifications in the global structural behaviour, which can be due, for instance, to earthquake-induced damage[36] or to retrofitting interventions[30].

This paper presents a vibration-based FE model updating procedure for historical masonry structures which have suffered severe damage due to seismic events, or other catastrophic events. First, this allows gathering further in-depth insights on the current condition of damaged buildings, which can reveal beneficial for the knowledge of their structural behaviour. Moreover, since masonry historical structures are highly vulnerable to seismic swarms (aftershocks can cause further damage due to the accumulated damage in masonry as well as to damage on the structure that exposes vulnerabilities[30]), a calibrated FE model of the structure representing the current behaviour is of great importance for the safety assessment with respect to aftershocks expected before the repairing.

This is also an important tool for the design of repairing and strengthening interventions. Finally, when it is necessary to perform seismic analyses (such as push-over analyses[37]) of the structure in its current (damaged) condition, mode shapes from the calibrated FE model can be required.

Such an updating procedure is tested on the main tower of the San Felice sul Panaro medieval fortress, which was heavily damaged by the 2012 Emilia earthquake. In particular, mechanical properties of the main tower and the level of connection with the rest of the fortress in the current damaged state are investigated based on the AVT performed after the earthquake. The FE mesh of the structure in its post-quake condition is generated by means of a non-standard mesh generation procedure called CLOUD2FEM, developed by some of the authors[12,38]. A 3D points cloud of the fortress, obtained by means of a laser scanner survey after

the Emilia earthquake, is semi-automatically transformed into a 3D FE mesh, allowing for a very accurate representation of the current geometry. Although the FE model accurately represents the geometry of the tower in the current state, the mechanical characteristics need to be calibrated with reference to the experimental results.

The methodology developed for the calibration of the FE model based on the experimentally identified modal parameters of the main tower is presented. To fully describe the actual behaviour of the main tower in operational conditions, mesh elements corresponding to the damaged masonry are identified and a different elastic modulus is assigned to them. This allows to account for the effect of damage and cracks in operational conditions and towards possible aftershocks, i.e. when the external actions are not such as to involve non-linear behaviour and damage and cracks only imply a local stiffness reduction. The FE model is calibrated adopting a surrogate-assisted evolutionary algorithm, namely the DE-S algorithm, proposed by one of the authors[39]. With the aim of reducing the computational effort, the algorithm combines an evolutionary strategy with a quadratic response surface to evaluate the structural parameters that potentially minimize the difference between numerical and experimental results.

The paper is organized as follows. First, the San Felice sul Panaro fortress is described in Section 2. Ambient vibration testing and modal parameter identification are presented in Section 3, while Section 4 describes the FE model of the fortress generated by means of the CLOUD2FEM procedure. Finally, the updating of the FE model using the DE-S algorithm is presented and discussed in Section 5.

2 | DESCRIPTION OF THE CASE-STUDY

The case under study is the main tower of the San Felice sul Panaro medieval fortress (Figure 1), located near the city of Modena. Such a tower is called Mastio because of its dominant dimensions compared to the rest of the building, see Figure 1 a. The tower, 32 m high with an almost square plan with sides of slightly more than 10 m, is composed of seven levels: three cross vaults and three timber decks as well as a timber trussed roof. The thickness of the tower trunk walls ranges from 2.5 m at the bottom up to 1.25 m at the top. Several openings of different sizes are irregularly placed along the tower. Furthermore, it is characterized by the presence of a crowning in its upper part which presents a larger plan, achieved through masonry corbels, which allows to enlarge the perimeter overhanging from the wall below. Along its West side, the tower is adjacent to the South entrance building, whereas in its North side it is linked to the curtain wall.

In 2012, the investigated structure was hit by the Emilia earthquake with two main shocks of magnitude $M_W = 5.86$ (May 20th) and $M_W = 5.66$ (May 29th)[40]. The epicentres of the first and the second main shocks were located at approximately ten and five kilometres far from San Felice sul Panaro, respectively. After the seismic sequence, the collapse of the four minor tower roofs was observed and cracks of different relevance appeared on all the fortress structural elements extensively, as shown in Figure 1 b. In[4], an accurate description of the Emilian medieval fortresses damage mechanisms is reported. Particularly, the Mastio most relevant damage consists in diagonal cracks, clearly visible in the lower half of the South and North front (Figures 2 a and 2 b). In order to prevent further collapses of the structure after the seismic sequence, the San Felice sul Panaro municipality commissioned first-aid safety interventions. In particular, the cracks of the main tower (and of the remaining structures) have been partially filled with lime and polyurethane (Figures 2 a and 2 b). Thereby, 15 mm diameter steel strands have been diffusely inserted into the main tower sections (highlighted with green circles in Figure 2 c), inside 60 mm large holes drilled into the walls and then grappled through lime mortar and pozzolan.

3 | MODAL IDENTIFICATION FROM AMBIENT RESPONSE

Ambient vibration tests were conducted on the Mastio of the San Felice sul Panaro fortress in July 2016, to measure the dynamic response in operational conditions and identify its modal properties. As the fortress was significantly damaged by the

2012 earthquake, the modal identification refers to the dynamic behaviour of the Mastio in damaged conditions.

The dynamic acquisition system was composed of 10 uni-axial piezoelectric accelerometers (7 PCB/393B12 and 3 PCB/393B31), with a dynamic range of ± 0.5 g, a bandwidth ranging form 0.15 to 1000 Hz and a resolution of 8 μg (PCB/393B12) and 1 μg (PCB/393B31). The accelerometers were connected to a National Instruments acquisition system for data storage and system management. The sampling frequency was set to 200 Hz. The response of the tower was measured simultaneously in 7 points belonging to 4 levels along the height of the main tower. In each measuring point, one or two accelerometers were placed, for a total of 10 measurement channels (A1-A10 in Figure 3). The accelerometers were installed on the inner walls by means of metal plates and screws, as shown in Figure 4 .

Figure 5 a presents a typical acceleration time series recorded at the upper instrumented level (L4). The measured acceleration ranges between ± 15 mg (corresponding to ± 0.15 m/s^2), stating the low level of ambient excitation during the test. The corresponding PSD function is shown in Figure 5 b. The modal identification is performed applying the Enhanced Frequency Domain Decomposition method to the acquired accelerations[41,42]. First, the Power Spectral Density (PSD) matrix of the acquired accelerations is calculated and decomposed with the Singular Value Decomposition (SVD) method. Each singular vector of the PSD matrix represents the *j*-th mode shape while the corresponding singular value is the amplification factor, i.e. the structural response amplification under dynamic loads. The *j*-th natural frequency is identified from the peak of the PSD graph. Finally, the damping ratio is estimated through the logarithmic decrement. The reader is referred to[41,42] for all the details about the method.

Table 1 presents the first five estimated natural frequencies and damping ratios while the corresponding mode shapes are shown in Figure 6 . Two closely-spaced modes are identified around 1.75 Hz. These modes are dominant bending and involve flexure in W-E direction (Figure 6 a) and N-S direction (Figure 6 b). The third mode mainly involves torsion of the main tower (Figure 6 c). The forth (Figure 6 d) and fifth (Figure 6 e) mode are characterized by dominant flexure in both directions. It can be observed that the modal displacement of the upper level (L4) often presents abnormalities compared to the lower levels. This behaviour may be related to (i) the significant damage of the masonry walls of the upper level and (ii) the fact that at the upper level sensors were mounted in different positions because of the different position of the masonry walls. Finally, damping ratios show values in the range [0.94% − 3.40%].

4 | FE MESH GENERATION AND NUMERICAL MODELLING

The FE model of the structure under study has been generated by means of a non-standard mesh generation procedure called CLOUD2FEM[12,38]. Such an innovative method semi-automatically transforms 3D points cloud of complex buildings into 3D FE meshes, minimizing the user-time investment. The procedure details are briefly revisited in this section as the FE mesh is used in the model updating process.

Given a points cloud, obtained by means of laser scanner or photogrammetric surveys of the inner and outer surfaces of a building, it can be processed by reducing the points density and by generating the Triangular Irregular Network (TIN) mesh, which is a standard routine. Such a mesh of the surfaces is broken down by means of a subdivision of the 3D domain into bi-dimensional sub-domains by slicing it perpendicularly to an opportune direction (typically the vertical direction) with a certain step. The slicing step is chosen according to the complexity of the building along the slicing direction. By using a concave hull algorithm[43], the boundary polygon that encloses the points of each slice is computed. Then, a filled region for each slice of the building is extracted and idealized as a digital image composed of pixels with a certain resolution. Such slices are stackable as the digitalization is performed on a fixed space region. The subsequent stacking of the slices generates voxels. Finally, each voxel is automatically transformed into an eight-node hexahedral finite element and, therefore, the structure

is completely discretized as an unique continuum composed by evenly spaced eight-node hexahedral elements.

As far as the investigated monument is concerned, the municipality of San Felice sul Panaro, after the first-aid safety interventions, commissioned a fine Terrestrial Laser Scanning (TLS) survey of the damaged building in order to acquire a snapshot of the after-quake structural condition, see Figure 7 . The surveyed raw points cloud (composed of over 40 millions of points) is shown in Figure 7 a, while the processed TIN mesh is shown in Figure 7 b. On this mesh, a slicing operation has been carried out, see Figure 7 c, using a vertical gap of $\Delta z = 25$ cm. 121 slices have been extracted and, after their processing with a concave hull algorithm, digitalized (see some examples in Figure 7 d) with a bi-dimensional resolution in the horizontal plane of 25cm×25cm, as suggested in [44].

Indeed, in [44] the authors carried out a natural frequencies comparison between different CLOUD2FEM-based mesh sizes of the main tower (as isolated tower), obtaining a very good performance of the 25cm×25cm×25cm mesh. Furthermore, the effectiveness of the meshing approach has been also investigated in [38] through a comparison with a very detailed CAD-based model. As a result, the resolution 25cm×25cm×25cm was found to be the best compromise between result accuracy and computational effort. In fact, although this mesh dimension does not accurately reproduce each small architectural detail, it guarantees a good accuracy in terms of global dynamic response having at least five hexahedral finite elements in the thickness of the main tower walls [12]. The resulting mesh, depicted in Figure 8 , is characterized by 409,300 hexahedral finite elements (each one 25cm×25cm×25cm) and 1,512,444 dofs.

It has to be pointed out that, although the laser scanner survey has been carried out on the damaged fortress, its capability to collect information about the cracks is substantially limited. Indeed, the chance of picking points in the depth of a crack is extremely challenging and strongly depends on the crack width and on the relative angle between the surveyed surface and the laser direction. Furthermore, most of the cracks was partially filled in the first-aid interventions. In addition, during the idealization of each slice as a digital image composed of 25cm-large pixels, every geometric detail smaller than this dimension is approximated.

Modelling the floors and vaults of monumental masonry structures has always been a challenging task [45]. In particular, it is commonly accepted that in order to perform 3D seismic analysis of masonry buildings, equivalent diaphragms can be used to model vaults [46]. In the adopted FE model, floors and vaults are automatically meshed by means of a jagged 3D representation of the original geometry and the mesh accuracy can be considered satisfactory aiming at the global structural response. Particularly, an isotropic elastic material has been assumed to roughly model deck timber elements with the values 8000 MPa, 2918 MPa and 415 kg/m^3 for Young's modulus, shear modulus and density, respectively [47].

The fortress was surrounded by a moat and, therefore, the outer ground level is approximately 3.5 m lower than the inner one. Accordingly, clamped boundary conditions have been applied in all the nodes located at the moat level, whereas the elements located within the courtyard have been modelled through an elastic continuum to coarsely take into account the presence of terrain. In particular, a linear elastic material with Young's modulus, shear modulus and density equal to 935 MPa, 316 MPa and 1200 kg/m^3 respectively, has been considered for terrain [48].

For the masonry elements, a linear elastic material with density and Poisson's ratio equal to 1800 kg/m^3 and 0.2, respectively, has been adopted. According to the Italian Codes [49], the Young's modulus of rubble masonry elements made of solid bricks and lime mortar is expected to lie in the range [850 MPa - 1250 MPa]. However, the actual value of the masonry elastic modulus is identified from the model updating procedure in Section 5.

Finally, roofing wooden structures have been considered as concentrated mass on the Mastio top elements, i.e. where the roof is borne.

Although in this study the attention is focused on the Mastio modal identification and model updating, the modelling of the whole fortress is considered essential by the authors as the tower under study is clearly non-isolated and the interaction between

adjacent structures can play a considerable role in the evaluation of natural frequencies and modal shapes. In particular, in [50,51] it arises that the stiffness of the adjacent parts and their mutual level of connection with the tower strongly influences its dynamic response. This aspect is further investigated in the following section. Therefore, by modelling the whole monument, the actual stiffness of the adjacent parts of the tower is directly accounted for.

To conclude, it has to be particularly stressed that the the adopted mesh generation approach directly considers the after-quake geometry of the structure, including for instance partial collapses, i.e. the configuration of the structure when the ambient vibration testing was carried out.

5 | MODEL UPDATING AND STRUCTURAL PARAMETER IDENTIFICATION

The FE model of the fortress is calibrated with respect to the experimental results so that the modal properties of the main tower agree as close as possible with the experimental ones. To this aim, a set of unknown structural parameters is evaluated from the minimization of an objective function defined as the difference between measured data and numerical predictions. Due to the complexity of the numerical model, the evaluation of numerical modal parameters is highly time consuming and the success of the optimization problem strongly depends on the efficiency of the optimization algorithm. Hence, an improved surrogate-assisted evolutionary strategy is adopted to reduce the number of objective function evaluations and find a compromise between local and global search. The optimization algorithm is described in Section 5.1 while the identification of the structural parameters is presented in Section 5.2.

5.1 | The DE-S algorithm

Genetic and evolutionary algorithms are widely used to solve global optimization problems. Their architecture is designed for large-scale problems and allows to avoid local minima. The main drawback is that a large number of function evaluations is often required to reach the convergence. Surrogate-assisted evolutionary strategies [52] use efficient computational models, such as Response Surfaces (RS), high polynomial functions or Kriging models [53], to approximate the objective function. They aim at evaluating those individuals that potentially have a good prediction of the objective function value. The introduction of a second-order surrogate in the Differential Evolution (DE) algorithm is proposed in [54].

In the DE-S algorithm, proposed by [39], a proper infill sampling strategy is introduced to further reduce the number of objective function evaluations. The candidate points are chosen trying to find a compromise between local and global search, i.e. enhancing both the accuracy in the region of the optimum predicted by the surrogate (local exploitation) and the global exploration. The DE-S algorithm is summarized in the following.

The optimization process is based on the simultaneous adoption of NP vectors $\mathbf{x}_{i,G}$, with $i = 1, ..NP$. Each vector $\mathbf{x}_{i,G}$ has dimension D, being D the number of unknown structural parameters, while G indicates the G-th population of vectors. First, the objective function values are evaluated for the initial population of vectors, randomly chosen in the search space. At each subsequent iteration and for each vector $\mathbf{x}_{i,G}$, a *trial vector* $\mathbf{v}_{i,G}$ is generated. To this aim, NP subsets of NS vectors are built, with $NS < NP$. Each subset contains the vector $\mathbf{x}_{i,G}$ and other $NS - 1$ vectors randomly selected among the remaining vectors of the G-th population. Each subset is used to calibrate a second-order response surface $\hat{H}$ as a local approximation of the objective function H:

$$\hat{H} = \frac{1}{2}\mathbf{x}^T\mathbf{Q}\mathbf{x} + \mathbf{L}^T\mathbf{x} + \beta_0 \tag{1}$$

where $\mathbf{Q}$ is a $D \times D$ coefficient matrix collecting the quadratic terms, $\mathbf{L}$ is a D-dimensional vector of linear terms and β_0 is a constant. Applying the least square estimation methods from the NS evaluated points, the parameters calibrating the RS model are evaluated. Depending on the shape of the approximating function $\hat{H}$, two possibilities occur. If the response surface is convex, the *mutant vector* $\mathbf{v}_{i,G}$ is defined as the minimizer $\mathbf{x}^*$ of the approximating

function, i.e.:

$$\mathbf{v}_{i,G} = \mathbf{x}^* = -\mathbf{Q}^{-1}\mathbf{L} \tag{2}$$

On the contrary, if the response surface is non-convex, the *mutant vector* $\mathbf{v}_{i,G}$ is obtained from the *Mutation* operation, based on a linear combination of vectors[55]:

$$\mathbf{v}_{i,G} = \mathbf{x}_{r_1,G} + F(\mathbf{x}_{r_2,G} - \mathbf{x}_{r_3,G}) \tag{3}$$

where r_1, r_2, r_3 are integer numbers randomly selected in the range $[1 - NP]$, with $r_1 \neq r_2 \neq r_3$, and F is a positive constant controlling the amplitude of the mutation, normally assumed smaller than 2. The *Crossover* operation is applied to increase the diversity of vectors and escaping local optima.

Each *mutant vector* represents a candidate for a new evaluation. For each candidate $\mathbf{v}_{i,G}$, the score is defined as the weighted sum of two criteria. The first one depends on the objective function value predicted by the surrogate. The second criterion depends on the distances of the candidate from the points where the objective function has been already evaluated.

The two scoring criteria are combined as follows:

$$W(\mathbf{v}_{i,G}) = w_R V_R(\mathbf{v}_{i,G}) + w_D V_D(\mathbf{v}_{i,G}) \tag{4}$$

where $V_R(\mathbf{v}_{i,G})$ and $V_D(\mathbf{v}_{i,G})$ are the scores and w_R and w_D the weights associated to the two criteria. Candidate points with low vales of W are preferred.

The score V_R depends on the objective function value predicted by the surrogate as follows:

$$V_R(\mathbf{v}_{i,G}) = 1 - e^{\frac{s_f^2}{H_{best} H_{min,s}}} \tag{5}$$

where s_f is the minimum of the quadratic approximation $\hat{H}$ (that is the minimum estimated by the surrogate), H_{best} is the best objective function value at the current iteration, while:

$$H_{min,s} = \min_{s=1,\ldots NS} H(\mathbf{x}_{s,G}) \tag{6}$$

is the minimum of the evaluations of the NS points ($\mathbf{x}_{s,G}$) selected for the calibration of the response surface.

The score V_D is derived from the distances of the candidate point to the points where the objective function has already been evaluated:

$$V_D(\mathbf{v}_{i,G}) = 1 - \frac{\Delta_{min}}{\Delta_{max}} \tag{7}$$

where Δ_{min} and Δ_{max} are the minimum and maximum weighted distances of the candidate point to the n points where the objective function is evaluated:

$$\Delta_{min} = \min_{p=1,..n} D(\mathbf{v}_{i,G}, \mathbf{x}_{p,G}) \tag{8}$$

$$\Delta_{max} = \max_{p=1,..n} D(\mathbf{v}_{i,G}, \mathbf{x}_{p,G}) \tag{9}$$

The weighted distances D are calculated from the Euclidean distances d and the objective function values as:

$$D(\mathbf{v}_{i,G}, \mathbf{x}_{i,G}) = d(\mathbf{v}_{i,G}, \mathbf{x}_{i,G}) \sqrt{\frac{H_{best}}{H(\mathbf{x}_{p,G})}} \tag{10}$$

The weights w_R and w_D are chosen in the range $0 \leq w \leq 1$, with $w_R + w_D = 1$. If w_D is close to 1, the global exploration prevails on the local one and candidate points placed in a rather unexplored region of the parameter domain are preferred. On the contrary, if w_R is high, candidate points with low objective function values are preferred (local exploitation).

Results of analyses performed in[39] suggest the adoption of the following weight factors: $w_R = 2/3$, $w_D = 1/3$ if the surrogate presents a minimum (case A in the flowchart of Figure 9) and $w_R = 0$, $w_D = 1$ when the surrogate search fails (case B). Indeed, in case A it is worth investigating the region close to the optimum predicted by the surrogate while in the second case the global exploration of the parameter domain is preferred.

To reduce the number of the objective function evaluations, a subset of NH candidates (with $NH < NP$) is selected. Candidates with the lowest score are preferred and only for this subset of points the objective function is evaluated. Finally, in the *Selection* operation, all points (candidates and points of the current population) are ordered depending on their objective function value. The NP points with the lowest value of the objective function are selected to be the members of the next population.

The flowchart of the DE-S algorithm is reported in Figure 9 . The reader is referred to[39] for all details about it.

5.2 | Identification of the structural parameters

The objective function H is a measure of the difference between numerical ($f_{num}, \boldsymbol{\phi}_{num}$) and experimental ($f_{sper}, \boldsymbol{\phi}_{sper}$) natural frequencies and mode shapes:

$$H(\mathbf{x}) = \sum_{j=1}^{N} \left[\alpha \left(\frac{f_{sper,j} - f_{num,j}}{f_{sper,j}} \right)^2 + (1-\alpha) \left(\frac{1 - \mathrm{MAC}(\boldsymbol{\phi}_{num,j}, \boldsymbol{\phi}_{sper,j})}{\mathrm{MAC}(\boldsymbol{\phi}_{num,j}, \boldsymbol{\phi}_{sper,j})} \right)^2 \right] \tag{11}$$

where α ($0 \leq \alpha \leq 1$) is a weighting factor that determines the relative importance between frequency and mode shape residuals, $\mathbf{x}$ is the vector of unknown structural parameters and N is the number of modes considered in the calibration procedure. Finally, MAC is the Modal Assurance Criterion[56], representing the correlation between two modal vectors.

First, it is important to identify which modes should be included in the calibration process. Indeed, in ambient vibration testing higher frequencies are often obtained with less accuracy than the lower order ones. Minimizing the error between experimental and numerical modal properties for higher modes may prevent matching the lower modes of vibration[57].

In this study, the first three natural modes (modes 1-3 in Table 1) are accounted for in the calibration procedure, whereas modes 4 and 5 are adopted for the purpose of validation of the updated FE model. This is in line with the fact that generally only the first natural modes are relevant for seismic analyses.

In[25], the influence of the weighting factor α on the identified structural parameters is investigated evaluating of the optimal solutions forming the Pareto front. Adopting two different selection criteria, an optimal value of α equal to 0.4 is obtained, although results are observed to be similar for α in the range $[0.1 - 0.8]$. Hence, in this study, the weighting factor α is set to 0.4.

Moreover, a proper selection of structural parameters is fundamental for the success of the calibration process. In particular, those parameters whose values are uncertain and that potentially have a considerable effect on the vibration response of the structure are to be selected.

The FE model of the fortress has been generated from the 3D points cloud obtained after a fine TLS survey of the fortress. This means that the physical dimensions of the masonry elements and floors are defined with reasonable accuracy. On the contrary, the material properties of the major structural components are more uncertain. Indeed, due to the serious damage of the fortress and its age of construction, the effective stiffness of the masonry is uncertain.

The first attempt to update the numerical model (**Model updating #1**) is carried out considering a homogeneous distribution of the masonry elastic properties. In particular, the structural parameter considered in the optimization procedure is the equivalent elastic modulus of the cracked masonry of the Mastio, indicated as E_M.

Table 2 presents the optimization analysis results, including the range of variation for each updating parameter and the identified value, the average frequency error and the average MAC value. The average frequency error and MAC value are calculated with reference to modes 1-3 and modes 4-5. The first are the natural modes against which the FE model is calibrated while the second are used to evaluate the goodness of fit of the calibrated model. The numerical frequency and MAC value for each natural mode are reported in Table 3 , together with a comparison to the experimental results. As far as the calibrated modes (1-3) are concerned, a pretty good match between numerical and experimental frequencies is obtained, with errors lower than 6%. Modes 1 and 3 show MAC values higher than 0.90, while a slightly lower correlation is observed for mode 2, characterized by a MAC value of 0.86. Larger differences between numerical and experimental results are obtained for modes 4 and 5, in relation to both natural frequencies (mode 4) and mode shapes (mode 5).

With regard to the identified structural parameters, an equivalent elastic modulus of the masonry of about 825 MPa is obtained. The identified value is lower than the expected one due to the presence of significant cracks in the masonry.

As the updated model does not describe the actual behaviour of the tower with respect to modes 4 and 5, additional structural parameters are accounted for in the optimization procedure. Due to the complex historical evolution of the fortress, its monolithic behaviour and the efficiency of connections between adjacent walls cannot be assured. Furthermore, some important damage can be observed in correspondence of the interfaces between the Mastio and the rest of the fortress. Therefore, the elastic moduli of the portions of walls connecting the Mastio to the fortress on the West (E_{CW}) and North (E_{CN}) side are considered as additional unknown parameters (highlighted in Figure 10).

A sensitivity analysis is performed to evaluate how each structural parameter influences the dynamic behaviour. The analysis is carried out varying the structural parameters one-by-one and setting the others to 825 MPa (i.e. the elastic modulus obtained from model updating #1). Figure 11 presents the value of the objective function evaluated from Eq.(11) as well as the partial contributions of natural frequency and mode shape residuals to the objective function. Figures 11 a and 11 b are obtained considering modes 1-3, while Figure 11 c considering modes 4 and 5.

As expected, the variation in the masonry elastic modulus E_M affects the natural frequencies and not the mode shapes (Figure 11 a). On the contrary, the variation in the elastic moduli E_{CW} and E_{CN} of the connection elements causes changes in modes shapes and slightly affects natural frequencies. In particular, the objective function values for different E_{CW} calculated considering modes 1-3 and modes 4-5 are reported in Figures 11 b and 11 c, respectively. When E_{CW} decreases, values of the objective function calculated from modes 1-3 increase while those calculated from modes 4-5 decrease. This highlights the non-negligible contribution of the interface element stiffness.

Hence, a second calibration (**Model updating #2**) is carried out considering as uncertain parameters the elastic modulus of the cracked masonry E_M and the elastic moduli of the connection elements E_{CW} and E_{CN}. The updated model shows an equivalent elastic modulus of the masonry equal to 932 MPa while the connection elements are characterized by low (<50 MPa) elastic moduli (Table 2). Compared to the model updating #1, the elastic modulus of masonry E_M increases to make up for the reduction of the connection stiffness. Moreover, the calibrated modes (modes 1-3) show a slight improvement in the mode shapes against a slight worsening in terms of natural frequencies. Similar to the model updating #1, a low correlation between experimental and numerical results is observed for modes 4 and 5.

From the previous calibrations, it follows that the equivalent elastic moduli of the cracked masonry is not the appropriate parameter to accurately characterize the Mastio dynamic behaviour. Indeed, the Mastio presents a severe crack pattern whose contribution cannot be accounted for simply defining an equivalent elastic modulus of the cracked masonry. To fully describe the actual behaviour of the main tower in operational conditions, an improvement of the FE model is proposed in this paper. After an accurate survey of damage and cracks, mesh elements corresponding to the damaged masonry are identified in the FE model (highlighted in Figure 12) and a different elastic modulus E_D is assigned to them. This allows to account for the effect of damage and cracks in operational conditions, i.e. when the external actions are not such as to involve nonlinear behaviour and damage and cracks only imply a local stiffness reduction. As the calibration is performed with reference to the modal properties of the Mastio, only the cracks of the Mastio are introduced in the FE model.

The third calibration process (**Model updating #3**) is carried out considering as unknown structural parameters the elastic moduli of the damaged E_D and undamaged E_U masonry. The updated model presents elastic moduli of the damaged and undamaged masonry equal to 700 MPa and 892 MPa, respectively (Table 2). As expected, the elastic modulus of the damaged masonry is lower than the one of the undamaged of masonry. However, the elastic modulus of the damaged masonry is representative of the cracks that, for the grater part, have been partially filled with lime and polyurethane after the 2012 earthquake. Once the FE model is improved accounting for the actually damaged portions of masonry, a much better consistency between numerical and experimental results is achieved. Indeed, the calibrated FE model presents frequency

errors between 3.51% and 7.72% and MAC values in the range $[0.75 - 0.95]$ for the five natural modes.

6 | CONCLUDING REMARKS

In this paper, a vibration-based model updating procedure for historical masonry structures which have suffered severe damage due to seismic events has been presented.

The methodology developed for the calibration of the numerical model, based on the experimentally identified modal parameters, has been carried out on the earthquake-damaged main tower of San Felice sul Panaro medieval fortress. The FE model of the structure in its post-quake condition has been generated by means of a non-standard semi-automatic mesh generation procedure. Ambient vibration testing was performed on the main tower of the fortress. Mechanical properties of the tower in its current damaged state have been investigated. To fully characterize the actual behaviour of the tower in operational conditions, mesh elements corresponding to the damaged masonry have been identified in the FE model and different material properties have been assigned to them, allowing to account for the effect of damage and cracks. This improvement was found to be fundamental aiming at consistently describing the dynamic behaviour of the tower in operational conditions by means of numerical modelling.

The updated FE model of the structure was able to guarantee a good accuracy of modal parameters of the concerned modes which were in close agreement with the experimental results, still preserving the physical meaning of updated parameters.

References

[1] W. Addis, *Building: 3000 years of design engineering and construction*, Phaidon Press, **2007**.

[2] E. Coïsson, D. Ferretti, E. Lenticchia, *Bulletin of Earthquake Engineering* **2017**, ., 1–28.

[3] C. Mazzotti, E. Sassoni, G. Pagliai, *Construction and Building Materials* **2014**, *54*, 421 – 431.

[4] S. Cattari, S. Degli Abbati, D. Ferretti, S. Lagomarsino, D. Ottonelli, A. Tralli, *Bulletin of Earthquake Engineering* **2014**, *12* (5), 2333–2365.

[5] C. Shermi, R.N. Dubey, *Construction and Building Materials* **2017**, *143*, 104 – 120.

[6] R. S. Nezhad, M. Z. Kabir, *Construction and Building Materials* **2017**, *131*, 630 – 640.

[7] A. Bilotta, F. Ceroni, E. Nigro, M. Pecce, *Construction and Building Materials* **2017**, *138*, 114 – 133.

[8] A. G. El-Attar, A. M. Saleh, A. H. Zaghw, *Structural Control and Health Monitoring* **2005**, *12* (2), 157–177.

[9] S. El-Borgi, H. Smaoui, F. Casciati, K. Jerbi, F. Kanoun, *Structural Control and Health Monitoring* **2005**, *12* (2), 179–195.

[10] C. A. Syrmakezis, *Structural Control and Health Monitoring* **2006**, *13* (6), 958–979.

[11] R. Maio, J. Estevao, T. M. Ferreira, R. Vicente, *Engineering Structures* **2017**, *141*, 41 – 58.

[12] G. Castellazzi, A. M. D'Altri, S. de Miranda, F. Ubertini, *Engineering Structures* **2017**, *132*, 229–248.

[13] C. Akcay, T. S. Bozkurt, B. Sayin, B. Yildizlar, *Construction and Building Materials* **2016**, *113*, 752 – 763.

[14] G. Boscato, R. Ceravolo, S. Russo, L. Zanotti Fragonara, *Computer-Aided Civil and Infrastructure Engineering* **2015**, *30* (8), 620–635.

[15] M. Betti, L. Galano, A. Vignoli, *Finite element modelling for seismic assessment of historic masonry buildings*, Sebastiano D'Amico (Ed.), Springer International Publishing, Cham, **2016**, pp. 377–415.

[16] A. De Stefano, R. Ceravolo, *Journal of Intelligent Material Systems and Structures* **2007**, *18*, 793–807.

[17] S. Podestà, G. Riotto, F. Marazzi, *Structural Control and Health Monitoring* **2008**, *15* (4), 622–641.

[18] A. Pau, F. Vestroni, *Structural Control and Health Monitoring* **2008**, *15* (8), 1105–1121.

[19] Ahmed Elyamani, Oriol Caselles, Pere Roca, Jaime Clapes, *Structural Control and Health Monitoring* **2017**, *24* (3), e1885–n/a, e1885 STC-15-0297.R1.

[20] K. A. Bani-Hani, H. S. Zibdeh, K. Hamdaoui, *Smart Structures and Systems* **2008**, *4* (2), 195–208.

[21] T. Demetriou, C. Chrysostomou, A. Stassis, *Smart Structures and Systems* **2008**, *4* (2), 183–194.

[22] A. J. Garcia-Palencia, E. Santini-Bell, J. D. Sipple, M. Sanayei, *Structural Control and Health Monitoring* **2015**, *22* (10), 1265–1281.

[23] J.L. Zapico, K. Worden, F.J. Molina, *Smart Materials and Structures* **2001**, *10* (3), 553.

[24] C.H. Chen, *Smart Materials and Structures* **2005**, *14* (3).

[25] M. Forghieri, E. Bassoli, L. Vincenzi, in *Proceedings of the 6th ECCOMAS Thematic Conference on Computational Methods in Structural Dynamics and Earthquake Engineering*, Rhodes Island, Greece, **2017**.

[26] A. D'Ambrisi, V. Mariani, M. Mezzi, *Engineering Structures* **2012**, *36*, 210 – 219.

[27] G. Russo, O. Bergamo, L. Damiani, D. Lugato, *Engineering Structures* **2010**, *32* (2), 353 – 360.

[28] S. Ivorra, F. J. Pallarés, *Engineering Structures* **2006**, *28* (5), 660 – 667.

[29] E. Bassoli, L. Vincenzi, M. Bovo, C. Mazzotti, in *Proceedings of the 2015 IEEE Workshop on Environmental, Energy and Structural Monitoring Systems*, Trento, Italy, **2015**.

[30] L. Zanotti Fragonara, G. Boscato, R. Ceravolo, S. Russo, S. Ientile, M. L. Pecorelli, A. Quattrone, *Bulletin of Earthquake Engineering* **2017**, *15* (1), 313–337.

[31] C. Gentile, A. Saisi, *Construction and Building Materials* **2007**, *21* (6), 1311 – 1321.

[32] L.F. Ramos, L. Marques, P.B. Lourenço, G. De Roeck, A. Campos-Costa, J. Roque, *Mechanical Systems and Signal Processing* **2010**, *24* (5), 1291 – 1305.

[33] L.F. Ramos, G. De Roeck, P.B. Lourenço, A. Campos-Costa, *Engineering Structures* **2010**, *32* (1), 146 – 162.

[34] R.A. Votsis, N. Kyriakides, C.Z. Chrysostomou, E. Tantele, T. Demetriou, *Soil Dynamics and Earthquake Engineering* **2012**, *43*, 58 – 68.

[35] A. Pau, F. Vestroni, *Mechanical Systems and Signal Processing* **2013**, *41* (1), 454 – 466.

[36] A. Saisi, C. Gentile, M. Guidobaldi, *Construction and Building Materials* **2015**, *81*, 101 – 112.

[37] S. Degli Abbati, A. M. D'Altri, D. Ottonelli, G. Castellazzi, S. Cattari, S. de Miranda, S. Lagomarsino, in *Proceedings of the 6th ECCOMAS Thematic Conference on Computational Methods in Structural Dynamics and Earthquake Engineering*, Rhodes Island, Greece, **2017**.

[38] G. Castellazzi, A. M. D'Altri, G. Bitelli, I. Selvaggi, A. Lambertini, *Sensors* **2015**, *15* (8), 18360–18380.

[39] L. Vincenzi, P. Gambarelli, *Computers and Structures* **2017**, *178*, 58–70.

[40] M. Savoia, N. Buratti, L. Vincenzi, *Engineering Structures* **2017**, *137*, 162 – 180.

[41] R. Brincker, L. Zhang, P. Andersen, *Smart Materials and Structures* **2001**, *10* (3), 441.

[42] R. Brinker, C. Ventura, P. Andersen, in *Proceedings of the 19th International Modal Analysis Conference*, San Antonio, Texas, USA, **2001**.

[43] A. Moreira, M.Y. Santos, in *Proceedings of the 2nd International Conference on Computer Graphics Theory and Applications*, Scitepress, **2007**.

[44] G. Castellazzi, A. M. D'Altri, S. de Miranda, F. Ubertini, G. Bitelli, A. Lambertini, I. Selvaggi, A. Tralli, in *ECCOMAS Congress 2016 - Proceedings of the 7th European Congress on Computational Methods in Applied Sciences and Engineering*, **2016**, pp. 409–416.

[45] A.M. D'Altri, G. Castellazzi, S. de Miranda, A. Tralli, *Journal of Building Engineering* **2017**, *13*, 224–243.

[46] S. Lagomarsino, S. Cattari, S. Resemini in *Structural Analysis of Historic Construction: Preserving Safety and Significance*, Informa UK Limited, **2008**, pp. 517–524.

[47] *DM 14/01/2008. Nuove norme tecniche per le costruzioni. Ministero delle Infrastrutture (GU n.29 04/02/2008), Rome, Italy [New technical norms on constructions, in italian].*

[48] M. Ghandil, F. Behnamfar, *Soil Dynamics and Earthquake Engineering* **2015**, *75*, 1 – 17.

[49] *Circolare 2009. Circolare n. 617 del 02/02/2009. Istruzioni per l'applicazione delle nuove Norme Tecniche per le Costruzioni di cui al D.M. del 14/01/2008 [in italian].*

[50] G. Castellazzi, A. M. D'Altri, S. de Miranda, S. Magagnini, A. Tralli, in *International Conference of Computational Methods in Sciences and Engineering 2016, ICCMSE 2016*, AIP Publishing, **2016**.

[51] G. Castellazzi, A. M. D'Altri, S. de Miranda, A. Chiozzi, A. Tralli, *Bullettin of Earthquake Engineering* **2017**, ., 1–29.

[52] Y. Jin, *Swarm and Evolutionary Computation* **2011**, *1* (2), 61 – 70.

[53] J. Müller, C.A. Shoemaker, R. Piché, *Computers & Operations Research* **2013**, *40* (5), 1383 – 1400.

[54] L. Vincenzi, M. Savoia, *Computer-Aided Civil and Infrastructure Engineering* **2015**, *30* (5), 376–393.

[55] R. Storn, K. Price, *Journal of Global Optimization* **1997**, *11*, 341–359.

[56] D. J. Ewins, *Modal testing: theory and practice*, John Wiley & Sons, New York, **2000**.

[57] X. Chen, P. Omenzetter, S. Beskhyroun, in *EWSHM - 7th European Workshop on Structural Health Monitoring*, (Eds: Vincent Le Cam, Laurent Mevel, Franck Schoefs), IFFSTTAR, Inria, Université de Nantes, Nantes, France, **2014**.

Mode n.	Mode type	Exp. Frequency [Hz]	Damping Ratio [%]
1	1^{st} Bending E-W	1.72	2.31
2	1^{st} Bending N-S	1.76	3.40
3	Torsional	3.55	2.24
4	2^{nd} Bending N-S	4.83	0.99
5	2^{nd} Bending E-W	5.08	0.94

TABLE 1 Experimental modes.

Model updating #1							
Structural parameter	Lower value	Upper value	Updated model	Average f error [%]		Average MAC	
				Modes 1-3	Modes 4-5	Modes 1-3	Modes 4-5
E_M [MPa]	500	1500	825	| 4.20 |	| 20.63 |	0.92	0.61
Model updating #2							
Structural parameter	Lower value	Upper value	Updated model	Average f error [%]		Average MAC	
				Modes 1-3	Modes 4-5	Modes 1-3	Modes 4-5
E_{CW} [MPa]	10	1500	38				
E_{CN} [MPa]	10	1500	12	| 5.16 |	| 32.95 |	0.94	0.76
E_M [MPa]	500	1500	931				
Model updating #3							
Structural parameter	Lower value	Upper value	Updated model	Average f error [%]		Average MAC	
				Modes 1-3	Modes 4-5	Modes 1-3	Modes 4-5
E_D [MPa]	10	1500	700	| 4.39 |	| 3.54 |	0.93	0.78
E_U [MPa]	500	1500	892				

TABLE 2 Parameters for structural identification and updated model.

Mode n.	Exp. Freq	Model updating #1			Model updating #2			Model updating #3		
		Num. Freq. [Hz]	Err. Freq. [%]	MAC [-]	Num. Freq. [Hz]	Err. Freq. [%]	MAC [-]	Num. Freq. [Hz]	Err. Freq. [%]	MAC [-]
1	1.72	1.81	-4.83	0.94	1.76	-2.43	0.95	1.78	-3.51	0.95
2	1.76	1.65	6.03	0.86	1.61	8.32	0.92	1.62	7.72	0.90
3	3.55	3.61	-1.75	0.94	3.71	-4.73	0.95	3.61	-1.94	0.94
4	4.83	6.41	-36.24	0.77	6.09	-29.46	0.77	4.84	-2.91	0.75
5	5.08	5.08	-5.01	0.45	6.60	-36.44	0.75	5.04	-4.16	0.81

TABLE 3 Experimental and numerical modes.

(a) (b)

Figure 1: San Felice sul Panaro fortress (a) before and (b) after the 2012 Emilia earthquake.

(a) (b) (c)

Figure 2: Mastio after the first-aid safety interventions: (a) South front, (b) North front and (c) particular of the injected steel strands.

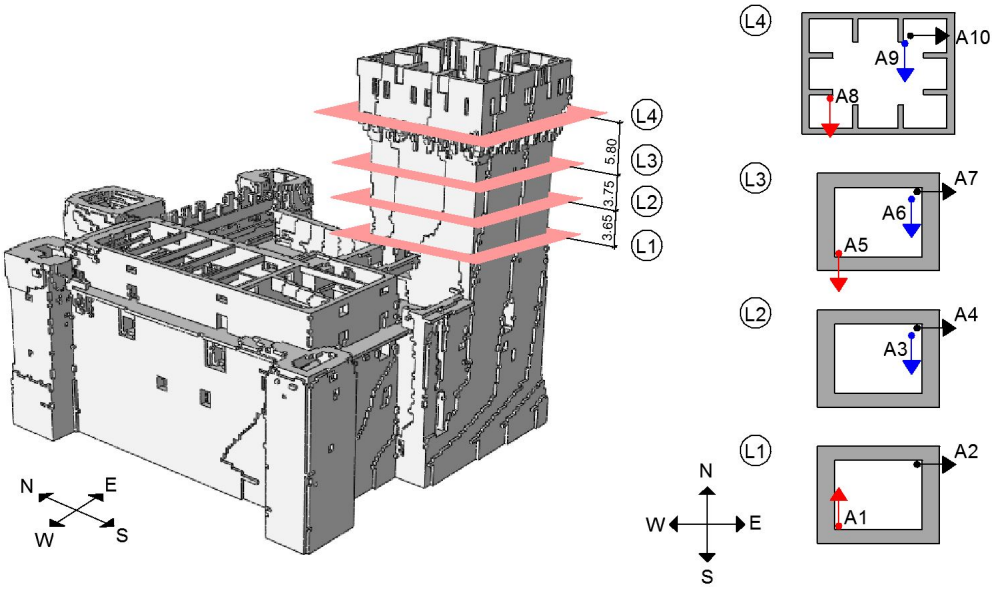

Figure 3: Instrumented levels (L1-L4) and layout of the accelerometers (A1-A10) during the ambient vibration testing.

(a) (b)

Figure 4: Typical installation of sensors.

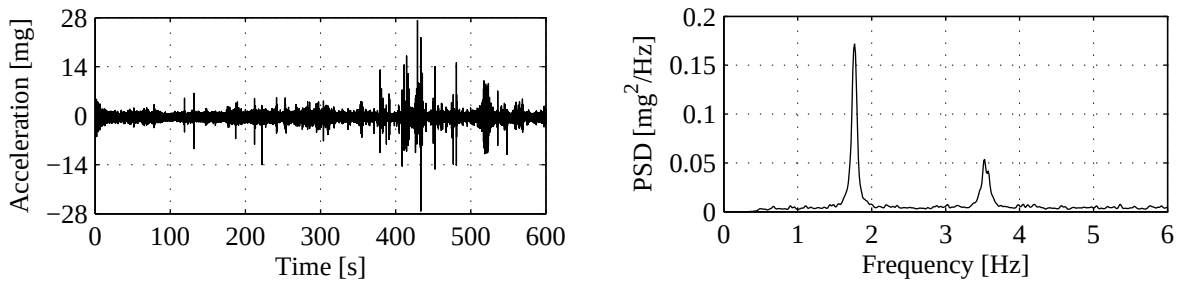

(a) (b)

Figure 5: (a) Typical time history of accelerations recorded at level L4 and (b) corresponding PSD function.

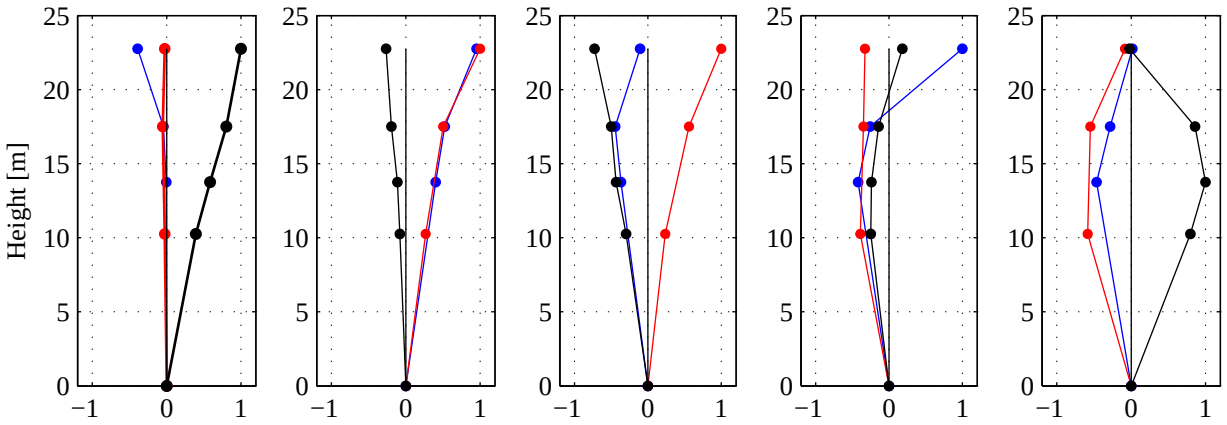

(a) Mode n.1 - f_1 = 1.72 Hz (b) Mode n.2 - f_2 = 1.75 Hz (c) Mode n.3 - f_3 = 3.55 Hz (d) Mode n.4 - f_4 = 4.83 Hz (e) Mode n.5 f_5 = 5.08 Hz

Figure 6: Mode shapes of the identified (a, b, d, e) bending and (c) torsional modes. Black: modal displacements of the measuring points in the N-E corner of the cross-section in E-W direction. Blue: modal displacement of the N-E corner in N-S direction. Red: modal displacement of the W-S corner in N-S direction.

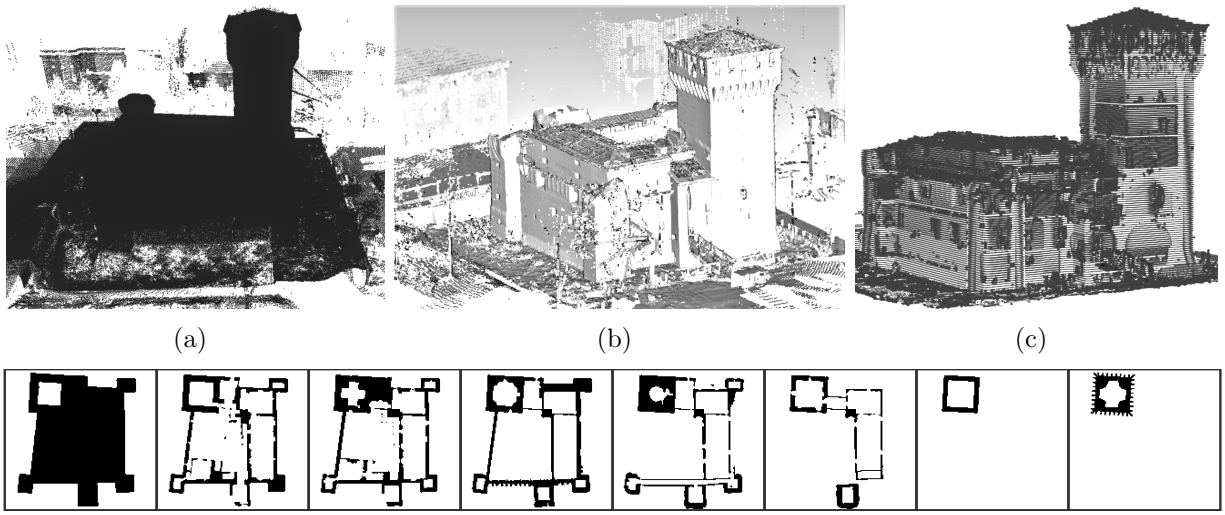

Figure 7: Fortress TLS survey processing: (a) points cloud (more than 40 millions of points), (b) TIN mesh (approximately 5 millions of triangles), (c) slicing of the TIN mesh and (d) some of the digitalized slices.

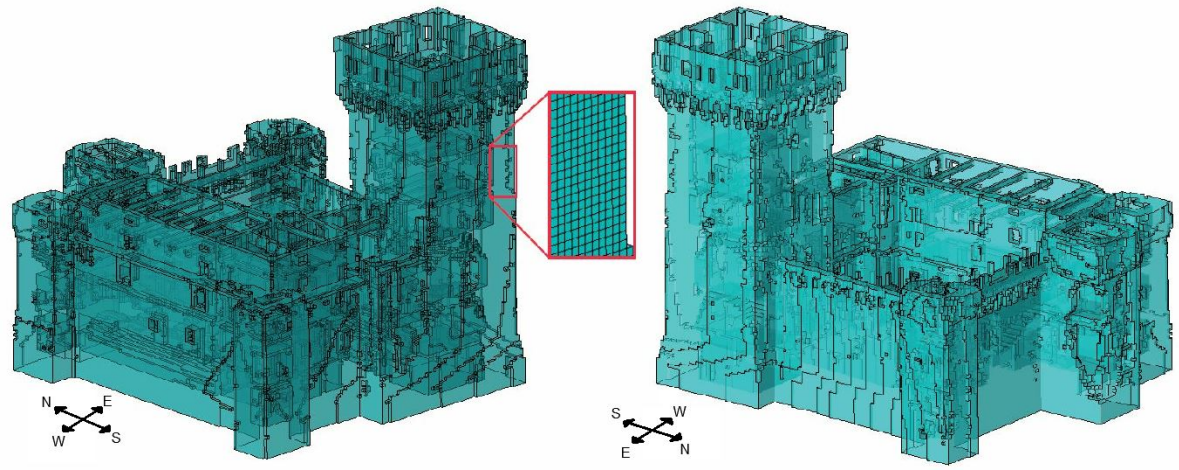

Figure 8: Generated FE model: the magnified portion shows the mesh discretization.

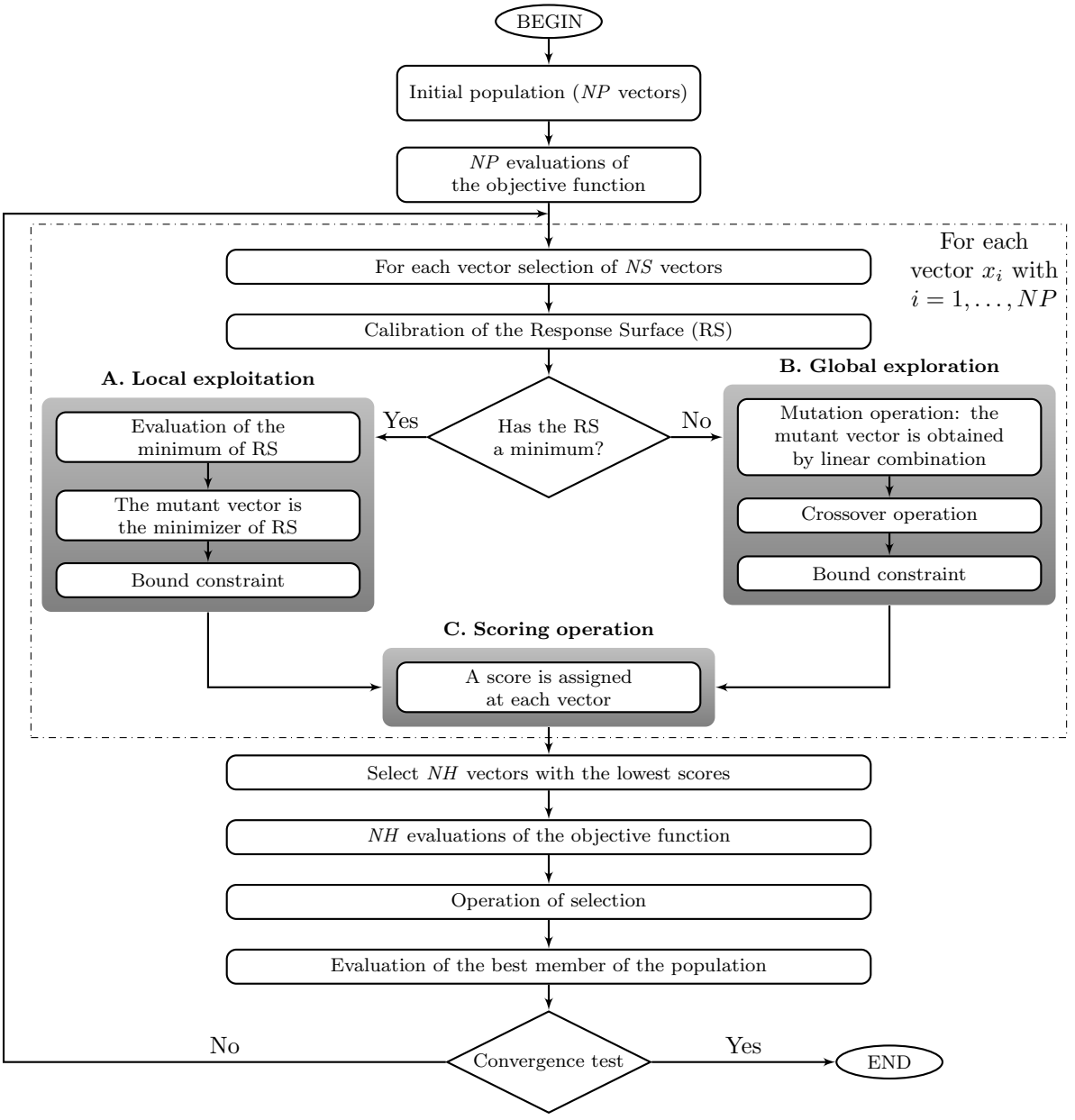

Figure 9: Flowchart of the DE-S algorithm.

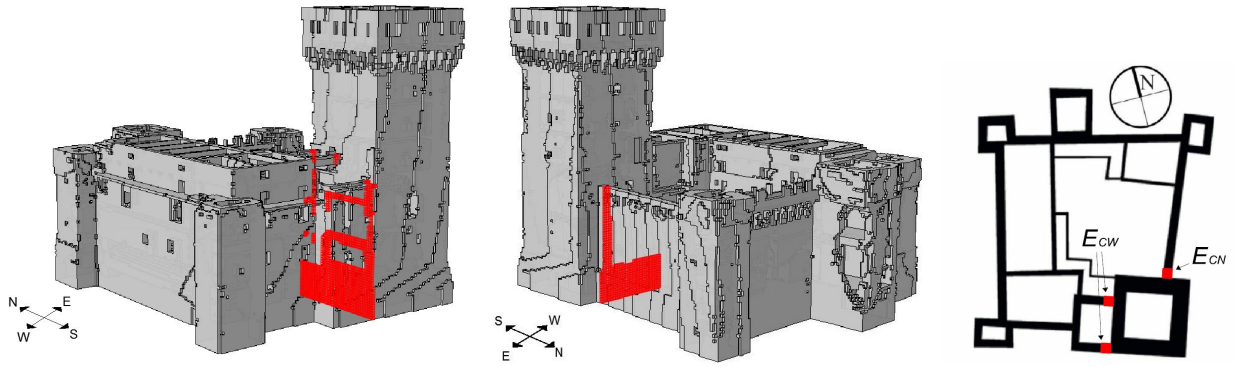

(a) (b) (c)

Figure 10: Highlighting of the elements connecting the main tower to the fortress on the (a) West and (b) North side and (c) a plan-view of the connection elements.

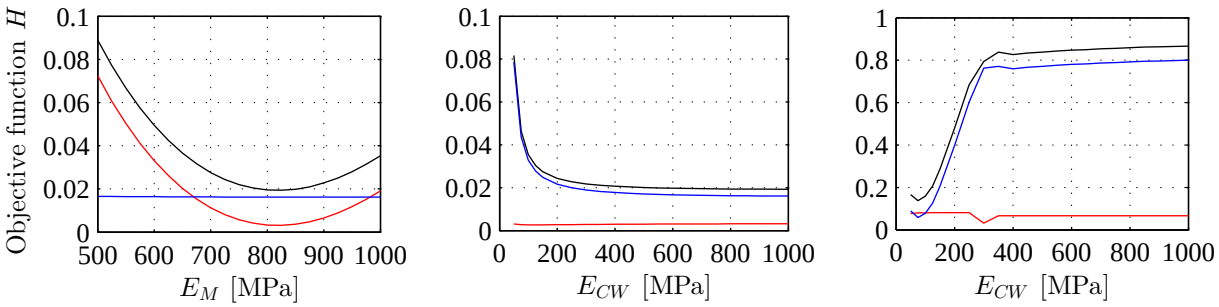

(a) modes 1-3 (b) modes 1-3 (c) modes 4-5

Figure 11: Sensitivity of the FE model to the elastic modulus of (a) the masonry and (b, c) the elements connecting the main tower to the fortress on the West side. Objective function in terms of both frequencies and mode shapes (black), only frequencies (red) and only mode shapes (blue).

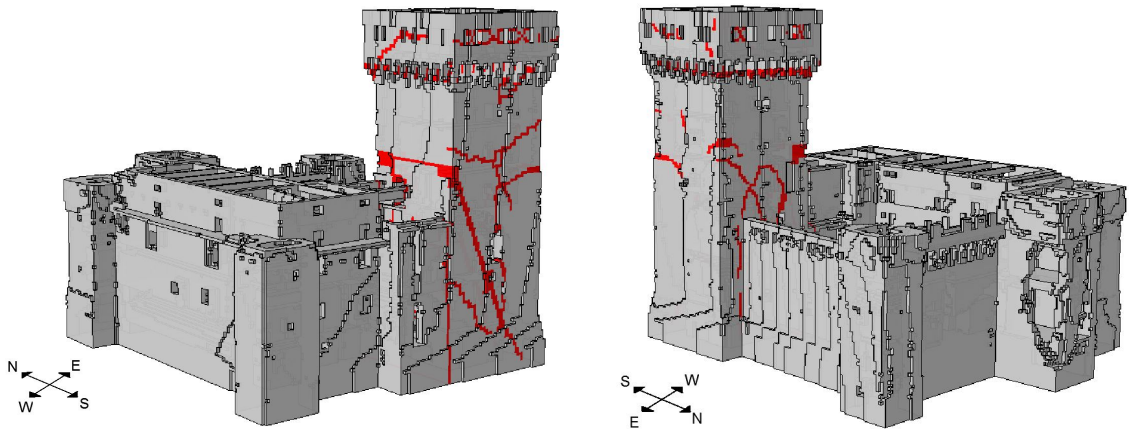

(a) (b)

Figure 12: Highlighting of the damaged elements (red).